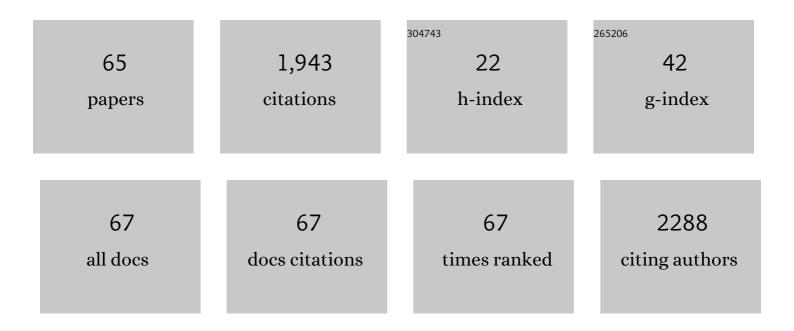


## List of Publications by Year in descending order

Source: https://exaly.com/author-pdf/2135547/publications.pdf Version: 2024-02-01



FEL XIA

#	Article	IF	CITATIONS
1	Identification of functional substates of KRas during GTP hydrolysis with enhanced sampling simulations. Physical Chemistry Chemical Physics, 2022, 24, 7653-7665.	2.8	9
2	Conformations and binding pockets of <scp>HRas</scp> and its guanine nucleotide exchange factors complexes in the guanosine triphosphate exchange process. Journal of Computational Chemistry, 2022, 43, 906-916.	3.3	9
3	Accurate and Efficient Estimation of Lennard–Jones Interactions for Coarse-Grained Particles via a Potential Matching Method. Journal of Chemical Theory and Computation, 2022, 18, 4879-4890.	5.3	5
4	CO <sub>2</sub> atmosphere enables efficient catalytic hydration of ethylene oxide by ionic liquids/organic bases at low water/epoxide ratios. Green Chemistry, 2021, 23, 3386-3391.	9.0	15
5	Dual Functional Pd-Catalyzed Multicomponent Reaction by Umpolung Chemistry of the Oxygen Atom in Electrophiles. Journal of Organic Chemistry, 2021, 86, 6847-6854.	3.2	5
6	Conformational Features of Ras: Key Hydrogen-Bonding Interactions of Gln61 in the Intermediate State during GTP Hydrolysis. Journal of Physical Chemistry B, 2021, 125, 8805-8813.	2.6	12
7	Iron speciation and annual records in black coral as new proxy for mining and environmental impacts. Science of the Total Environment, 2021, 776, 145965.	8.0	1
8	Ammonium promoting methane oxidation by stimulating the Type Ia methane-oxidizing bacteria in tidal flat sediments of the Yangtze River estuary. Science of the Total Environment, 2021, 793, 148470.	8.0	5
9	Determining Optimal Coarseâ€Grained Representation for Biomolecules Using Internal Cluster Validation Indexes. Journal of Computational Chemistry, 2020, 41, 14-20.	3.3	9
10	Double-Well Ultra-Coarse-Grained Model to Describe Protein Conformational Transitions. Journal of Chemical Theory and Computation, 2020, 16, 6678-6689.	5.3	20
11	Alcohol amine-catalyzed CO <sub>2</sub> conversion for the synthesis of quinazoline-2,4-(1 <i>H</i> ,3 <i>H</i> )-dione in water. RSC Advances, 2020, 10, 34910-34915.	3.6	9
12	Reaction Mechanism of CO <sub>2</sub> and Styrene Oxide Catalyzed by Ionic Liquids: A Combined DFT Calculation and Experimental Study. Journal of Physical Chemistry A, 2020, 124, 7991-7998.	2.5	3
13	How CuCl and CuCl <sub>2</sub> Insert into C–N Bonds of Diazo Compounds: An Electronic Structure and Mechanistic Study. Journal of Physical Chemistry A, 2020, 124, 2029-2035.	2.5	5
14	DNA nanotweezers for stabilizing and dynamically lighting up a lipid raft on living cell membranes and the activation of T cells. Chemical Science, 2020, 11, 1581-1586.	7.4	16
15	Ir-catalyzed tandem hydroformylation-transfer hydrogenation of olefins with (trans-/cis-)formic acid as hydrogen source in presence of 1,10-phenanthroline. Journal of Catalysis, 2020, 385, 183-193.	6.2	12
16	Coarse-Grained Simulation of Mechanical Properties of Single Microtubules With Micrometer Length. Frontiers in Molecular Biosciences, 2020, 7, 632122.	3.5	6
17	Highly Regioselective Radical Transformation of <i>N</i> -Sulfonyl-1,2,3-triazoles in Air. Organic Letters, 2019, 21, 6413-6417.	4.6	23
18	Mechanistic Studies of CO2 Cycloaddition Reaction Catalyzed by Amine-Functionalized Ionic Liquids. Frontiers in Chemistry, 2019, 7, 615.	3.6	20

**Γει Χι**α

#	Article	IF	CITATIONS
19	Diastereoselective synthesis of 3,3-disubstituted 3-nitro-4-chromanone derivatives as potential antitumor agents. Organic and Biomolecular Chemistry, 2019, 17, 1062-1066.	2.8	12
20	A new method for the construction of coarse-grained models of large biomolecules from low-resolution cryo-electron microscopy data. Physical Chemistry Chemical Physics, 2019, 21, 9720-9727.	2.8	6
21	Specific Substates of Ras To Interact with GAPs and Effectors: Revealed by Theoretical Simulations and FTIR Experiments. Journal of Physical Chemistry Letters, 2018, 9, 1312-1317.	4.6	23
22	Imidazolium ionic liquids/organic bases: Efficient intermolecular synergistic catalysts for the cycloaddition of CO2 and epoxides under atmospheric pressure. Molecular Catalysis, 2018, 446, 124-130.	2.0	45
23	Co-catalysis over a bi-functional ligand-based Pd-catalyst for tandem bis-alkoxycarbonylation of terminal alkynes. Green Chemistry, 2018, 20, 2588-2595.	9.0	34
24	Combination of transition metal Rh-catalysis and tautomeric catalysis through a bi-functional ligand for one-pot tandem methoxycarbonylation-aminolysis of olefins towards primary amides. Journal of Catalysis, 2018, 361, 230-237.	6.2	6
25	Conformer-related pathways in cycloaddition of vinylaziridines and alkynes catalyzed by rhodium(I)-complex. Chemical Physics Letters, 2018, 713, 21-25.	2.6	2
26	Ubiquity and Diversity of Complete Ammonia Oxidizers (Comammox). Applied and Environmental Microbiology, 2018, 84, .	3.1	146
27	Electrostatic Polarization Effect on Cooperative Aggregation of Full Length Human Islet Amyloid. Journal of Chemical Information and Modeling, 2018, 58, 1587-1595.	5.4	2
28	A triple-functionalised metal centre-catalyzed enantioselective multicomponent reaction. Organic Chemistry Frontiers, 2018, 5, 2799-2804.	4.5	11
29	Performance Comparison of Systematic Methods for Rigorous Definition of Coarse-Grained Sites of Large Biomolecules. Journal of Chemical Information and Modeling, 2017, 57, 214-222.	5.4	6
30	A Rh(II)-catalyzed multicomponent reaction by trapping an α-amino enol intermediate in a traditional two-component reaction pathway. Science Advances, 2017, 3, e1602467.	10.3	42
31	Deactivating Influence of 3- <i>O</i> -Glycosyl Substituent on Anomeric Reactivity of Thiomannoside Observed in Oligomannoside Synthesis. Journal of Organic Chemistry, 2017, 82, 2599-2621.	3.2	9
32	Construction of ultra-coarse-grained model of protein with a Gŕlike potential. Chemical Physics Letters, 2017, 681, 1-6.	2.6	10
33	A DFT calculation-inspired Rh( <scp>i</scp> )-catalyzed reaction via suppression of α-H shift in α-alkyldiazoacetates. Chemical Science, 2017, 8, 4312-4317.	7.4	28
34	Highly Fluorescent Polyimide Covalent Organic Nanosheets as Sensing Probes for the Detection of 2,4,6-Trinitrophenol. ACS Applied Materials & Interfaces, 2017, 9, 13415-13421.	8.0	234
35	An improved protocol with a highly degenerate primer targeting copper-containing membrane-bound monooxygenase genes for community analysis of methane- and ammonia-oxidizing bacteria. FEMS Microbiology Ecology, 2017, 93, fiw244.	2.7	35
36	Origins of Protons in C–H Bond Insertion Products of Phenols: Proton-Self-Sufficient Function via Water Molecules. Journal of Physical Chemistry A, 2017, 121, 6523-6529.	2.5	8

**Γει Χι**α

#	Article	IF	CITATIONS
37	A theoretical study of the substituent effect on reactions of amines, carbon dioxide and ethylene oxide catalyzed by binary ionic liquids. RSC Advances, 2017, 7, 51521-51527.	3.6	11
38	Tagged Highly Degenerate Primer (THDP)-PCR for Community Analysis of Methane- and Ammonia-oxidizing Bacteria Based on Copper-containing Membrane-bound Monooxygenases (CuMMO). Bio-protocol, 2017, 7, e2354.	0.4	0
39	A new algorithm for construction of coarse-grained sites of large biomolecules. Journal of Computational Chemistry, 2016, 37, 795-804.	3.3	18
40	Constructing Optimal Coarse-Grained Sites of Huge Biomolecules by Fluctuation Maximization. Journal of Chemical Theory and Computation, 2016, 12, 2091-2100.	5.3	19
41	DFT Calculations on the Mechanism of Transition-Metal-Catalyzed Reaction of Diazo Compounds with Phenols: O–H Insertion versus C–H Insertion. Journal of Physical Chemistry A, 2016, 120, 6485-6492.	2.5	45
42	Reaction mechanisms of carbon dioxide, ethylene oxide and amines catalyzed by ionic liquids BmimBr and BmimOAc: a DFT study. Physical Chemistry Chemical Physics, 2016, 18, 27951-27957.	2.8	22
43	DBU and DBUâ€Derived Ionic Liquid Synergistic Catalysts for the Conversion of Carbon Dioxide/Carbon Disulfide to 3â€Arylâ€2â€oxazolidinones/[1,3]Dithiolanâ€2â€ylidenephenyl―amine. ChemCatChem, 2016, 8, 8	302-8738.	74
44	Mechanistic Investigation of Aromatic C(sp <sup>2</sup> )–H and Alkyl C(sp <sup>3</sup> )–H Bond Insertion by Gold Carbenes. Journal of Physical Chemistry A, 2016, 120, 1925-1932.	2.5	29
45	Origins of unique gold-catalysed chemo- and site-selective C–H functionalization of phenols with diazo compounds. Chemical Science, 2016, 7, 1988-1995.	7.4	118
46	Communities of ammonia oxidizers at different stages of Spartina alterniflora invasion in salt marshes of Yangtze River estuary. Journal of Microbiology, 2015, 53, 311-320.	2.8	19
47	Bond cleavage, fragment modification and reassembly in enantioselective three-component reactions. Nature Communications, 2015, 6, 5801.	12.8	86
48	Enantioselective gold-catalyzed intermolecular [2+2] <i>versus</i> [4+2]-cycloadditions of 3-styrylindoles with <i>N</i> -allenamides: observation of interesting substituent effects. Chemical Science, 2015, 6, 5564-5570.	7.4	106
49	Construction of unique six-coordinated titanium species with an organic amine ligand in titanosilicate and their unprecedented high efficiency for alkene epoxidation. Chemical Communications, 2015, 51, 9010-9013.	4.1	107
50	Complete genome sequence of Methylophilus sp. TWE2 isolated from methane oxidation enrichment culture of tap-water. Journal of Biotechnology, 2015, 211, 121-122.	3.8	9
51	Heterogeneous elastic network model improves description of slow motions of proteins in solution. Chemical Physics Letters, 2015, 618, 102-107.	2.6	7
52	Identifying essential pairwise interactions in elastic network model using the alpha shape theory. Journal of Computational Chemistry, 2014, 35, 1111-1121.	3.3	17
53	An Ylide Transformation of Rhodium(I) Carbene: Enantioselective Threeâ€Component Reaction through Trapping of Rhodium(I)â€Associated Ammonium Ylides by βâ€Nitroacrylates. Angewandte Chemie - International Edition, 2014, 53, 13136-13139.	13.8	90
54	Combined effect of confinement and affinity of crowded environment on conformation switching of adenylate kinase. Journal of Molecular Modeling, 2014, 20, 2530.	1.8	7

**Γει Χι**α

#	Article	IF	CITATIONS
55	Robust Heterogeneous Anisotropic Elastic Network Model Precisely Reproduces the Experimental B-factors of Biomolecules. Journal of Chemical Theory and Computation, 2013, 9, 3704-3714.	5.3	18
56	Multiscale Coarse-Graining via Normal Mode Analysis. Journal of Chemical Theory and Computation, 2012, 8, 4797-4806.	5.3	16
57	Detailed Structure of the H <sub>2</sub> PO <sub>4</sub> <sup>–</sup> –Guanosine Diphosphate Intermediate in Ras-GAP Decoded from FTIR Experiments by Biomolecular Simulations. Journal of the American Chemical Society, 2012, 134, 20041-20044.	13.7	33
58	Ras and GTPase-activating protein (GAP) drive GTP into a precatalytic state as revealed by combining FTIR and biomolecular simulations. Proceedings of the National Academy of Sciences of the United States of America, 2012, 109, 15295-15300.	7.1	75
59	The Role of Magnesium for Geometry and Charge in GTP Hydrolysis, Revealed by Quantum Mechanics/Molecular Mechanics Simulations. Biophysical Journal, 2012, 103, 293-302.	0.5	46
60	The specific vibrational modes of GTP in solution and bound to Ras: a detailed theoretical analysis by QM/MM simulations. Physical Chemistry Chemical Physics, 2011, 13, 21451.	2.8	27
61	Base-Catalyzed Peptide Hydrolysis Is Insensitive to Mechanical Stress. Journal of Physical Chemistry B, 2011, 115, 10126-10132.	2.6	17
62	Minimum energy compact structures in force-quench polyubiquitin folding are domain swapped. Proceedings of the National Academy of Sciences of the United States of America, 2011, 108, 6963-6968.	7.1	16
63	Reaction Mechanisms for Câ^'O Bond Coupling from Pt <sub>4</sub> CH <sub>2</sub> <sup>+</sup> and O <sub>2</sub> :  A Relativistic Density Functional Study. Organometallics, 2007, 26, 6076-6081.	2.3	5
64	Relativistic density-functional study on the dehydrogenation reactivity of PtMCH2+(M=Cu,Ag,Au,Pt) toward NH3. Chemical Physics Letters, 2006, 418, 386-391.	2.6	22
65	Density Functional Characterization of Reactions of Bimetallic Carbenes PtMCH2+(M = Pt, Au) with NH3in the Cas Phase. Organometallics. 2005. 24. 1845-1851	2.3	17